European Radiology (2019) 29:3241–3252
https://doi.org/10.1007/s00330-018-5958-1

MUSCULOSKELETAL

Diffusion tensor imaging of the sciatic nerve in Charcot–Marie–Tooth disease type I patients: a prospective case–control study

Hyun Su Kim[1] · Young Cheol Yoon[1,2] · Byung-Ok Choi[3] · Wook Jin[4] · Jang Gyu Cha[5] · Jae-Hun Kim[1]

Received: 3 October 2018 / Revised: 19 November 2018 / Accepted: 5 December 2018 / Published online: 11 January 2019

Abstract

Objectives This study aimed to evaluate whether diffusion tensor imaging (DTI) parameters and cross-sectional area (CSA) can differentiate between the sciatic nerve of Charcot–Marie–Tooth (CMT) disease type I (demyelinating form) patients and that of controls.

Methods This prospective comparison study included 18 CMT type I patients and 18 age/sex-matched volunteers. Magnetic resonance imaging including DTI and axial T2-weighted Dixon sequence was performed for each subject. Region of interest analysis was independently performed by two radiologists on each side of the sciatic nerve at four levels: hamstring tendon origin (level 1), lesser trochanter of the femur (level 2), gluteus maximus tendon insertion (level 3), and mid-femur (level 4). Fractional anisotropy (FA), mean diffusivity (MD), axial diffusivity (AD), and radial diffusivity (RD) were calculated. The CSA of the sciatic nerve bundle was measured using axial water-only image at each level. Comparisons of DTI parameters between the two groups were performed using the two-sample *t* test and Mann–Whitney *U* test. Interobserver agreement analysis was also conducted.

Results Interobserver agreement was excellent for all DTI parameter analyses. FA was significantly lower at all four levels in CMT patients than controls. RD, MD, and CSA were significantly higher at all four levels in CMT patients. AD was significantly higher at level 2 in CMT patients.

Conclusion DTI assessment of the sciatic nerve is reproducible and can discriminate the demyelinating nerve pathology of CMT type I patients from normal nerves. The CSA of the sciatic nerve is also a potential parameter for diagnosing nerve abnormality in CMT type I patients.

Key Points

- *Diffusion tensor imaging parameters of the sciatic nerve at proximal to mid-femur level revealed significant differences between the Charcot–Marie–Tooth disease patients and controls.*
- *The cross-sectional area of the sciatic nerve was significantly larger in the Charcot–Marie–Tooth disease patients.*
- *Interobserver agreement was excellent (intraclass coefficient > 0.8) for all diffusion tensor imaging parameter analyses.*

Keywords Diffusion tensor imaging · Magnetic resonance imaging · Neuromuscular disease · Sciatic nerve

Electronic supplementary material The online version of this article (https://doi.org/10.1007/s00330-018-5958-1) contains supplementary material, which is available to authorized users.

✉ Young Cheol Yoon
youngcheol.yoon@gmail.com; ycyoon@skku.edu

[1] Department of Radiology, Samsung Medical Center, School of Medicine, Sungkyunkwan University, 81 Ilwon-Ro, Gangnam-gu, Seoul 135-710, South Korea

[2] Department of Health Sciences and Technology, SAIHST, Sungkyunkwan University, Seoul, South Korea

[3] Department of Neurology, Samsung Medical Center, School of Medicine, Sungkyunkwan University, Seoul, South Korea

[4] Department of Radiology, Kyung Hee University Hospital at Gangdong, Seoul, South Korea

[5] Department of Radiology, Soonchunhyang University Bucheon Hospital, Bucheon, South Korea

Abbreviations

AD	Axial diffusivity
CMT	Charcot–Marie–Tooth disease
CSA	Cross-sectional area
DTI	Diffusion tensor imaging
FA	Fractional anisotropy
MD	Mean diffusivity
MRI	Magnetic resonance imaging
RD	Radial diffusivity
ROC	Receiver operating characteristic
ROI	Region of interest

Introduction

Charcot–Marie–Tooth disease (CMT) is among the most common hereditary neuromuscular disorders, which are a genetically and phenotypically heterogeneous group of disorders [1, 2]. It includes hereditary disorders associated with motor and sensory deficits of the peripheral nervous system characterized by symmetric distal predominant muscle wasting, weakness, and sensory loss [1]. This symptom is most evident in the lower limbs and slowly progresses in a lengthdependent manner [3]. CMT is classically divided into two types: the more common type I, the demyelinating form, characterized by a slow nerve conduction velocity (NCV), and type II, the axonal form, with only normal or slightly reduced NCV but mainly reduced amplitude of motor and sensory responses in neurographic recordings [3].

CMT is most often diagnosed clinically, but it may go unrecognized before overt clinical features such as pes cavus or hammer toe become evident because of its insidious onset [1, 4]. Imaging studies are increasingly being conducted, which may aid in the evaluation of CMT patients. Reported imaging findings of the nerve structure in CMT patients have revealed nerve hypertrophy with fascicular swelling [5–8]. Muscle change as a result of denervation, which represents a more advanced stage and is more evident on magnetic resonance imaging (MRI), has recently attracted clinical interest [9–12]. Beyond this, little attention has been paid to the evaluation of peripheral nerves in CMT patients and quantitative analysis of imaging parameters.

Diffusion tensor imaging (DTI) is an emerging imaging technology that exploits the capability of MRI to obtain directional information of water molecule diffusion within biologic tissue. Using the anisotropic diffusion property of nerve tissue, DTI can provide useful quantitative data such as fractional anisotropy (FA) or mean diffusivity (MD) [13, 14]. With these parameters, DTI has been reported to have great potential in the assessment of degeneration and regeneration in nerve structure [15]. Axial diffusivity (AD) and radial diffusivity (RD), which represent diffusivity parallel and perpendicular to the orientation of the fiber, respectively, are also promising DTI parameters which may have high clinical value [16]. Studies have shown that these parameters are related to axonal and myelin sheath integrity [16–18]. DTI was initially applied in brain imaging, but recently, numerous studies on its application in peripheral nerve imaging have obtained promising results [19–21]. However, limited data have been collected for DTI application in peripheral nerves other than the median nerve [22].

We hypothesized that DTI parameters can reveal the difference between the demyelinated sciatic nerves of CMT type I patients and the normal sciatic nerves of healthy controls. Thus, we sought to determine the potential value of DTI in diagnosing sciatic neuropathy by performing a prospective comparison study encompassing CMT type I patients and healthy controls. We also hypothesized that cross-sectional area (CSA) of the sciatic nerves significantly differs between the two groups, so their measurements were performed.

Materials and methods

Study population

The sample size needed to detect meaningful differences in the mean FA of the sciatic nerve between the CMT type I and control groups was prospectively calculated with an alpha value of 0.05 and a beta value of 0.2. The expected difference in FA between the two groups was assumed to be 0.1 (standard deviation, 0.1) based on the results of a previous study [23]. The sample size (N) was calculated using the following equation: $N = 2(1.96 + 0.84)^2\sigma^2/\delta^2$, where σ and δ are the standard deviation of FA and the expected mean difference of FA between the two groups, respectively. The calculated sample size for each group was 16. The expected dropout rate was set at 10%, and therefore, the number of patients per group was 18.

Between February and June 2017, 18 patients with CMT type I, diagnosed through genetic analysis and electrophysiologic study (Supplementary Tables 1 and 2), underwent prospective MRI. Seventeen patients who underwent genetic analysis were diagnosed as CMT type IA. They all had peripheral myelin protein 22 (PMP22) duplication. One patient who did not undergo genetic testing was diagnosed with CMT type I based on clinical history and electrophysiologic study results suggesting severe demyelinating sensorimotor polyneuropathy. The cohort was limited to patients aged between 20 and 40 years (mean age, 30.1 years ± 4.3 years; age range, 23–37 years; 8 males and 10 females). None of the patients had other neuromuscular disorder or diabetes. They had no contraindication to MRI, such as claustrophobia or metal in the body. Patients were enrolled on a first-come, first-served basis.

A public notice was posted on a bulletin board at our institution to recruit 18 age- and sex-matched healthy controls with no history of peripheral neuropathy or pathologic condition related to the lower extremities, or contraindications to MRI.

The desired ages and sex distribution were included in the public notice, and 18 people volunteered (Supplementary Table 3).

A neurologist with 21 years of experience performed a physical examination to assess for signs of neurologic abnormality before MRI. All 18 age- and sex-matched controls (mean age, 28.2 years ± 1.2 years; age range, 20–36 years; 8 males and 10 females) revealed no neurologic abnormality on physical examination.

Investigational review board approval was obtained for the study, and all patients and volunteers gave written informed consent prior to MRI. No dropout occurred in either the study or control group, and therefore, the data obtained from 18 patients in each group were used for analysis.

MRI acquisition

MRI images were acquired using a 3.0-T MRI system (Ingenia; Philips Healthcare) and a 16-channel anterior coil and posterior built-in coil. After localization, the following MRI sequences were obtained for morphologic imaging of the patients: axial T1-weighted turbo spin-echo sequences (TR/TE, 450–650/15 ms; section thickness, 2 mm; intersection gap, 1 mm; field of view, 350 × 350 mm; acquisition matrix, 320 × 320; imaging time, 162 s; number of slices, 67), coronal T1-weighted turbo spin-echo sequences (TR/TE, 450–650/15 ms; section thickness, 5 mm; intersection gap, 0.5 mm; field of view, 350 × 350 mm; acquisition matrix, 320 × 320; imaging time, 200 s; number of slices, 25), and axial T2-weighted Dixon sequences (TR/TE, 4635.5/80 ms; section thickness, 2 mm; intersection gap, 1 mm; field of view, 350 × 350; acquisition matrix, 320 × 320; imaging time, 194 s; number of slices, 67). Water-only, fat-only, in-phase, and out-of-phase images were obtained from the Dixon sequences.

DTI was performed using single-shot echo planar imaging and the inversion recovery technique for fat suppression (TR/TE, 7576.4/78.5 ms; section thickness, 3 mm; no intersection gap; field of view, 350 × 350; acquisition matrix, 128 × 128;

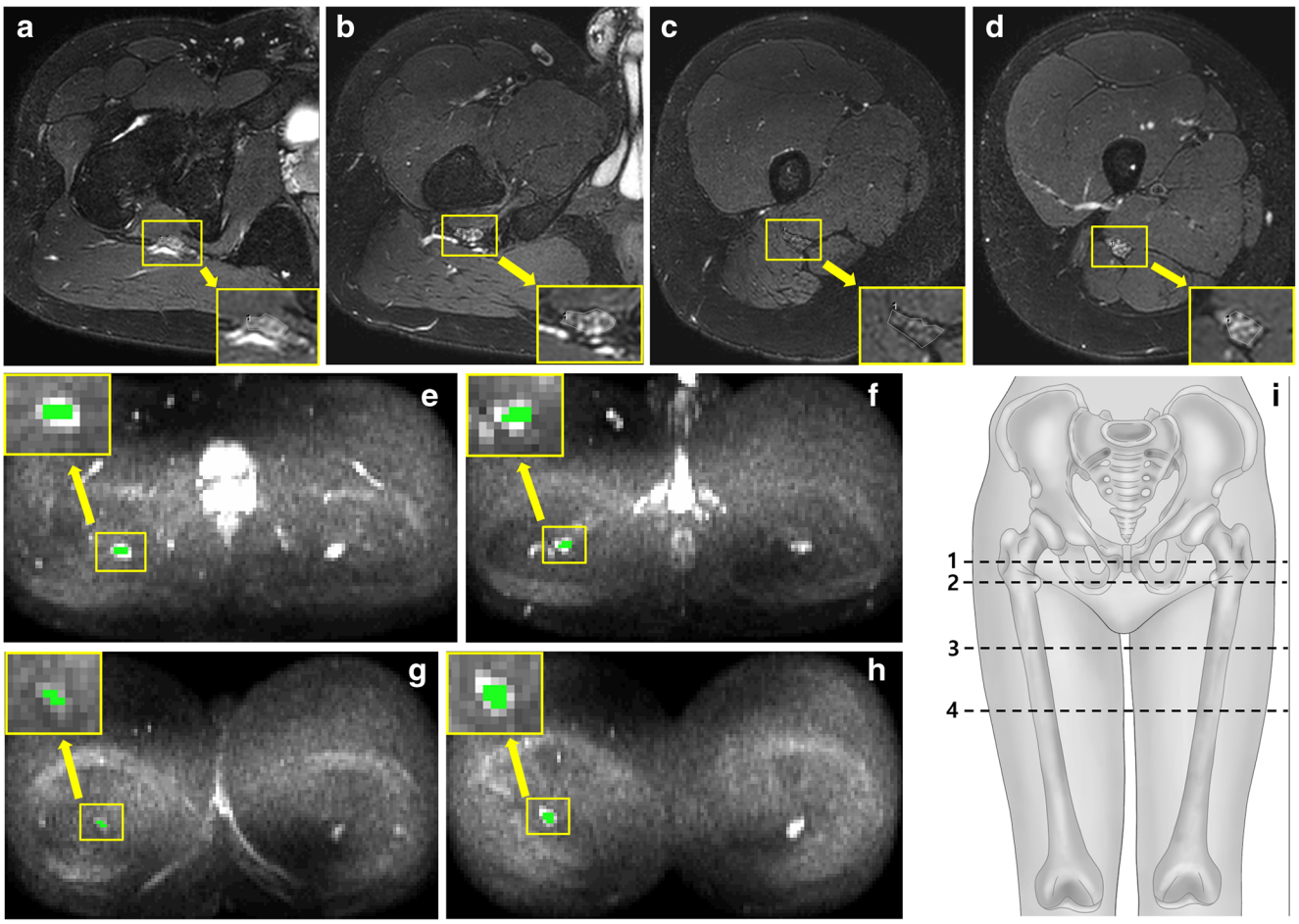

Fig. 1 An example of region of interest (ROI) analyses of the sciatic nerve in a 24-year-old male Charcot–Marie–Tooth disease type I patient. Axial Dixon water-only images (**a**–**d**) and the b_{800} maps (**e**–**h**) where the ROI analyses of the sciatic nerve were performed: hamstring tendon origin (**a**, **e**, level 1), lesser trochanter of the femur (**b**, **f**, level 2), gluteus maximus tendon insertion (**c**, **g**, level 3), and mid-femur (**d**, **h**, level 4). A magnified image of the ROI at each level is shown in the corner. Chosen pixels within the right sciatic nerve were marked green on the b_{800} maps (**e**–**h**) using designated software. An illustration (**i**) depicts the four levels where ROI analyses were performed

imaging time, 651.6 s; number of slices, 67; and delta [time from the center of the first gradient to the center of the second gradient]/delta [plateau duration of the diffusion gradient], 39.5/27.1 ms). Images were obtained at levels from the anterior inferior iliac spine through the distal femur in the axial plane. Parallel imaging was performed using sensitivity encoding (SENSE; Philips Healthcare). Diffusion gradients were applied in six directions with *b* values of 0 and 800 s/mm^2. Diffusion encoding was done with monopolar gradient pulses.

Data analysis

First, two radiologists evaluated the DTI image quality by consensus, which was defined by several factors, including motion artifact and diagnostic acceptability. A 4-point scale was used: 1, *very poor image quality*; 2, *suboptimal image quality*; 3, *mild limitation in image quality but no loss of pathology*; and 4, *optimal*. Grades 3 and 4 were considered acceptable.

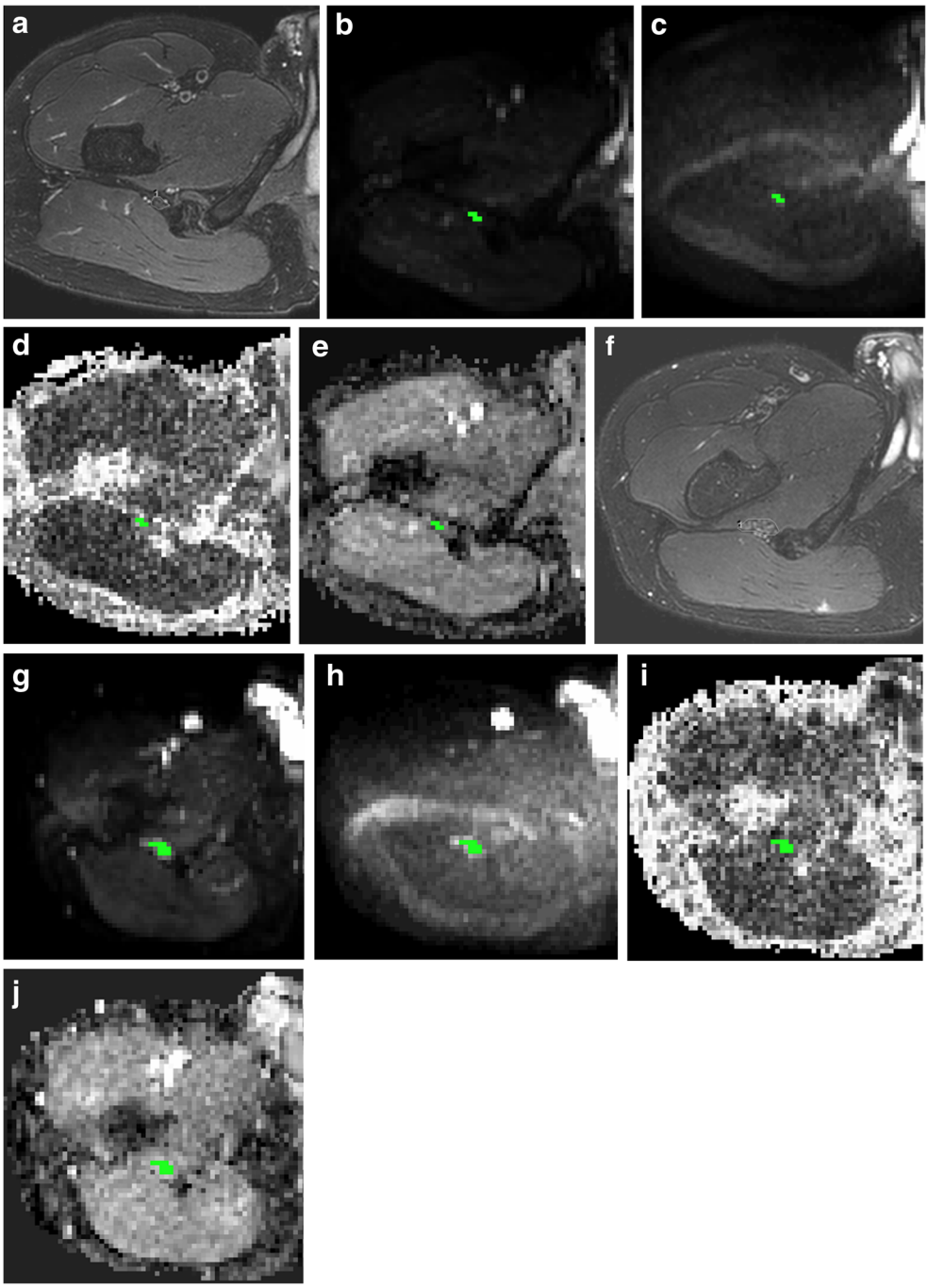

Fig. 2 An example of region of interest (ROI) analysis of the sciatic nerve in a 25-year-old male volunteer (**a**–**e**) and a 26-year-old male Charcot–Marie–Tooth disease type I patient (**f**–**j**). ROIs along the boundary of the right sciatic nerve for cross-sectional area measurement at level 2 in the water-only image (**a**, **f**). Chosen pixels marked green within the right sciatic nerve at level 2 in b_0 map (**b**, **g**), b_{800} map (**c**, **h**), fractional anisotropy map (**d**, **i**), and mean diffusivity map (**e**, **j**)

The dcm2nii tool (www.nitrc.org/projects/dcm2nii/) was used to convert the DICOM images to NIfTI format and extract the diffusion gradient directions. Parametric maps of FA, AD, RD, and MD were calculated using the Diffusion Toolkit software (www.trackvis.org/dtk) to generate diffusion maps. Region of interest (ROI) analysis was independently performed by two radiologists (Y.C.Y. and H.S.K., with 14 years and 5 years of experience in musculoskeletal radiology, respectively), using the MRIcro® software (www.mricro.com, version 1.4) on a b_{800} map. To clarify the position of the sciatic nerve on DTI, axial, b_0 map, and coronal T1 and T2 water-only images displayed on separate monitors were used as a reference. ROIs were drawn on each side of the sciatic nerve at four levels (Figs. 1 and 2): hamstring tendon origin (level 1), where the uppermost part of the semimembranosus tendon is visualized; lesser trochanter of the femur (level 2) , where it is visualized most prominently; gluteus maximus tendon insertion (level 3), where the uppermost part of the tendon insertion is visualized; and mid-femur (level 4), determined using a cross-reference tool and coronal images. A single slice of image was chosen for analysis at each level, and ROIs were carefully drawn pixel-by-pixel to fall within the visualized boundary of the nerve. Considering the limited resolution, signal-to-noise ratio, and small caliber of the nerve, ROI analysis was not performed at the distal thigh level. A training session was conducted in advance of measurement to familiarize both radiologists with the areas of measurement and defining ROI for the sciatic nerves. One radiologist (H.S.K., with 5 years of experience in musculoskeletal radiology) measured the CSA of the sciatic nerve bundle on water-only images at each level where DTI parameters were measured. Axial T1-weighted images were referred to in order to confirm the boundary of the nerve bundle.

Statistical analysis

Statistical analyses were performed using SAS (version 9.4; SAS Institute). Interobserver agreement regarding DTI was calculated using intraclass correlation coefficients, interpreted as follows: 0.8–1.0, *excellent*; 0.6–0.8, *good*; and < 0.6, *poor agreement*.

The DTI parameters and CSA of the sciatic nerve in the CMT patients and controls were compared at each level using two-sample *t* tests or Mann–Whitney *U* tests, as appropriate. Data of the left and right sciatic nerves were averaged together for comparison. The absence of laterality effect was confirmed in all the parameters by Mann–Whitney *U* tests (Supplementary Table 4). Comparison of body mass index (BMI) between the two groups was conducted using the Mann–Whitney *U* test to confirm the presence of a significant difference that may affect CSA of the sciatic nerve. Normality of data distribution was assessed using the Kolmogorov–Smirnov test. A p value < 0.05 was considered significant.

Receiver operating characteristic (ROC) curve analyses were performed for the parameters with mean values differing significantly between the two groups to evaluate their performance as a discriminator of normal and pathologic sciatic nerves. The optimal cutoff value of each parameter was determined using the Youden index. On the basis of the optimal cutoff value, the area under the curve (AUC) sensitivity, specificity, accuracy, and positive and negative predictive values were evaluated for each parameter.

Table 1 Interobserver agreement in diffusion tensor imaging analyses

	FA		AD		RD		MD	
	ICC	95% CI	ICC	95% CI	ICC	95% CI	ICC	95% CI
Level 1								
Right	0.91	0.83–0.95	0.90	0.90–0.90	0.92	0.92–0.92	0.93	0.91–0.91
Left	0.93	0.87–0.97	0.93	0.93–0.93	0.89	0.89–0.89	0.91	0.90–0.90
Level 2								
Right	0.96	0.92–0.98	0.88	0.88–0.88	0.95	0.95–0.95	0.90	0.93–0.93
Left	0.95	0.90–0.97	0.94	0.94–0.94	0.96	0.96–0.96	0.93	0.96–0.96
Level 3								
Right	0.92	0.84–0.96	0.96	0.96–0.96	0.96	0.96–0.96	0.96	0.96–0.96
Left	0.96	0.92–0.98	0.97	0.97–0.97	0.98	0.98–0.98	0.96	0.98–0.98
Level 4								
Right	0.92	0.85–0.96	0.96	0.96–0.96	0.92	0.92–0.92	0.98	0.94–0.94
Left	0.92	0.86–0.96	0.95	0.95–0.95	0.92	0.93–0.93	0.94	0.94–0.94

ICC intraclass coefficient, *CI* confidence interval, *FA* fractional anisotropy, *AD* axial diffusivity, *RD* radial diffusivity, *MD* mean diffusivity

Table 2 Comparison of diffusion tensor imaging parameters and cross-sectional area for healthy controls and Charcot–Marie–Tooth disease type I patients

	FA			AD			RD		
	Controls	CMT patients	*p* value	Controls	CMT patients	*p* value	Controls	CMT patients	*p* value
Level 1	0.549 ± 0.098	0.373 ± 0.208	< 0.0001*	$2.384 \times 10^{-3} \pm 0.319 \times 10^{-3}$	$2.400 \times 10^{-3} \pm 0.238 \times 10^{-3}$	0.8158	$0.892 \times 10^{-3} \pm 0.210 \times 10^{-3}$	$1.304 \times 10^{-3} \pm 0.293 \times 10^{-3}$	< 0.0001*
Level 2	0.549 ± 0.087	0.370 ± 0.093	< 0.0001*	$2.161 \times 10^{-3} \pm 0.194 \times 10^{-3}$	$2.286 \times 10^{-3} \pm 0.299 \times 10^{-3}$	0.0446*	$0.982 \times 10^{-3} \pm 0.389 \times 10^{-3}$	$1.364 \times 10^{-3} \pm 0.234 \times 10^{-3}$	< 0.0001*
Level 3	0.628 ± 0.108	0.455 ± 0.124	< 0.0001*	$2.118 \times 10^{-3} \pm 0.291 \times 10^{-3}$	$2.129 \times 10^{-3} \pm 0.394 \times 10^{-3}$	0.9003	$0.731 \times 10^{-3} \pm 0.220 \times 10^{-3}$	$1.098 \times 10^{-3} \pm 0.369 \times 10^{-3}$	< 0.0001*
Level 4	0.586 ± 0.118	0.484 ± 0.090	0.0002*	$2.238 \times 10^{-3} \pm 0.334 \times 10^{-3}$	$2.381 \times 10^{-3} \pm 0.375 \times 10^{-3}$	0.1083	$0.885 \times 10^{-3} \pm 0.250 \times 10^{-3}$	$1.141 \times 10^{-3} \pm 0.249 \times 10^{-3}$	< 0.0001*

	RD	MD			CSA		
	p value	Controls	CMT patients	*p* value	Controls	CMT patients	*p* value
Level 1	< 0.0001*	$1.445 \times 10^{-3} \pm 0.289 \times 10^{-3}$	$1.699 \times 10^{-3} \pm 0.204 \times 10^{-3}$	< 0.0001*	43.510 ± 14.468	85.100 ± 39.347	< 0.0001*
Level 2	< 0.0001*	$1.315 \times 10^{-3} \pm 0.187 \times 10^{-3}$	$1.631 \times 10^{-3} \pm 0.286 \times 10^{-3}$	< 0.0001*	48.723 ± 17.076	95.119 ± 36.564	< 0.0001*
Level 3	< 0.0001*	$1.194 \times 10^{-3} \pm 0.212 \times 10^{-3}$	$1.442 \times 10^{-3} \pm 0.369 \times 10^{-3}$	0.0050*	39.003 ± 14.383	90.794 ± 36.664	< 0.0001*
Level 4	< 0.0001*	$1.336 \times 10^{-3} \pm 0.240 \times 10^{-3}$	$1.554 \times 10^{-3} \pm 0.256 \times 10^{-3}$	0.0008*	29.277 ± 10.598	88.839 ± 41.708	< 0.0001*

Data are displayed as mean values ± standard deviation

FA fractional anisotropy, *AD* axial diffusivity, *RD* radial diffusivity, *MD* mean diffusivity, *CSA* cross-sectional area

*Statistically significant

Fig. 3 Boxplots for the comparison of diffusion tensor imaging parameters and cross-sectional area for healthy controls and Charcot–Marie–Tooth disease type I patients. Single asterisk indicates significant difference between the two groups. *CMT* Charcot–Marie–Tooth disease, *FA* fractional anisotropy, *AD* axial diffusivity, *RD* radial diffusivity, *MD* mean diffusivity, *CSA* cross-sectional area. Empty circles indicate outliers

Results

After the two radiologists evaluated the DTI image quality by consensus, images of three of the controls were rated as grade 2 (suboptimal image quality) and were consequently excluded. The other DTI images were considered acceptable (8 at grade 3; 25 at grade 4).

Interobserver agreement was excellent for all DTI parameter analyses (Table 1), and data obtained by one of the reviewers was used for comparison. FA values were significantly lower at all four measured levels in the CMT patients compared with those of the controls (Table 2, Fig. 3). RD, MD, and CSA were significantly higher at all four measured levels in the CMT patients compared with those of the controls. AD was significantly higher at level 2 in the CMT patients. There was no significant difference of BMI between the two groups ($p = 0.270$; volunteers: median ± standard deviation, 21.60 ± 3.09; interquartile range, 20.60–25.10; CMT patients: median ± standard deviation, 23.06 ± 4.99; interquartile range, 21.48–27.63).

Overall diagnostic performance for parameters at varying level is shown in Table 3. The highest AUC was 0.921 (level 1) for FA, 0.865 (level 2) for RD, 0.815 (level 2) for MD, and 0.932 (level 3) for CSA. The AUC was 0.651 (level 2) for AD. FA showed sensitivity of 94.4% and specificity of 90.0% at level 1. Cutoff values for each parameter were 0.435–0.559 for FA, 0.955×10^{-3}–1.222×10^{-3} for RD, 1.350×10^{-3}–1.564×10^{-3} for MD, 50.0–64.0 for CSA, and 2.398×10^{-3} for AD.

Discussion

In this study, the DTI parameters obtained from analysis of the sciatic nerve differed significantly between CMT type I patients and controls. At all four measured levels, FA was significantly lower while MD and RD were significantly higher in CMT patients than in volunteers. The diagnostic performance of the parameters at each level for discriminating CMT patients and controls with cutoff values was provided, which may be used as a reference in the future studies. All parameters showed high inter-rater reproducibility. These results may imply a feasibility for clinical application of DTI in the evaluation of the sciatic nerve in CMT type I patients and, possibly, in patients with other types of demyelinating neuropathy.

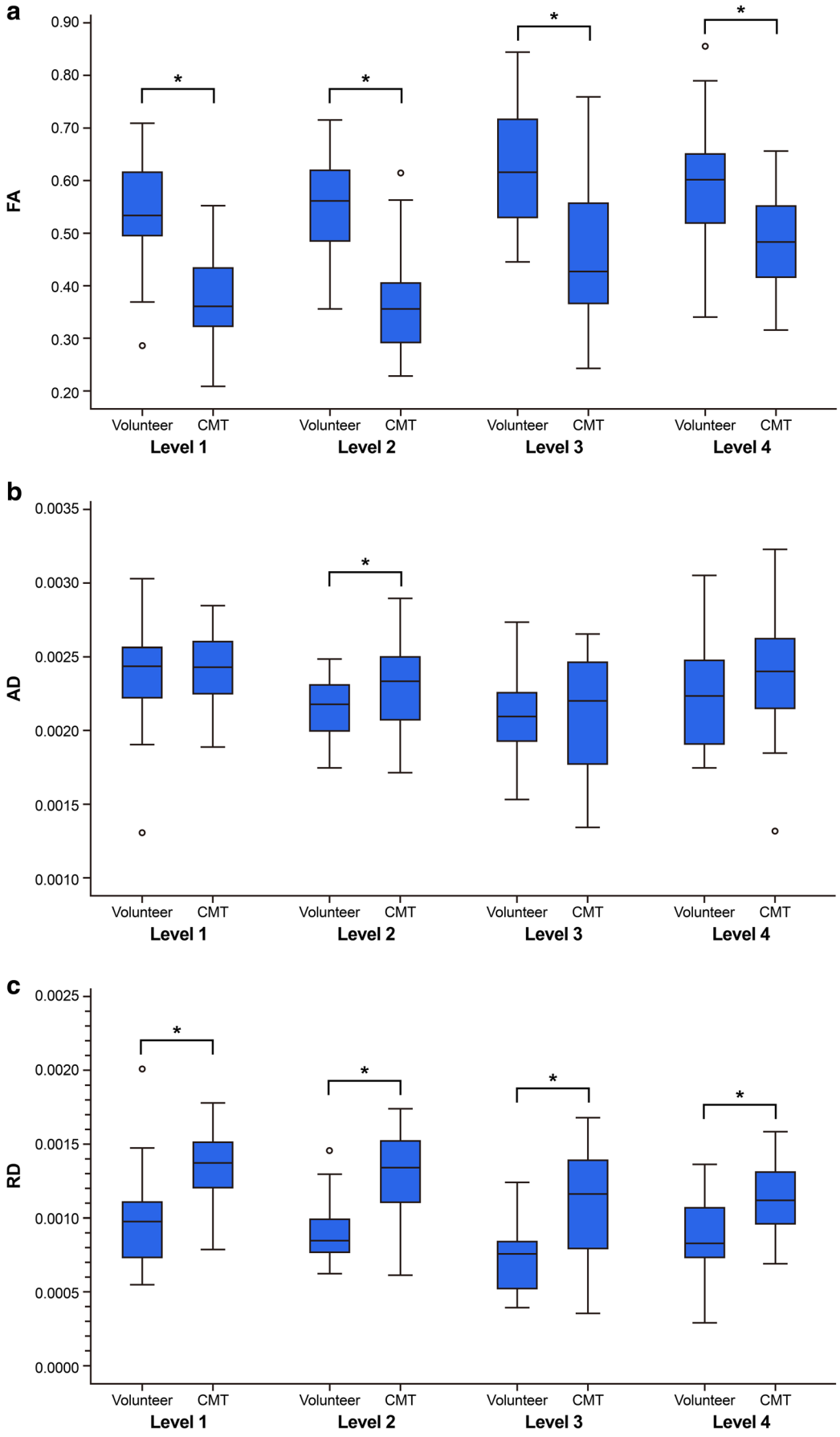
a
FA
0.90
0.80
0.70
0.60
0.50
0.40
0.30
0.20
*
Volunteer
CMT
Level 1
Level 2
Level 3
Level 4
b
AD
0.0035
0.0030
0.0025
0.0020
0.0015
0.0010
c
RD
0.0025
0.0020
0.0015
0.0010
0.0005
0.0000

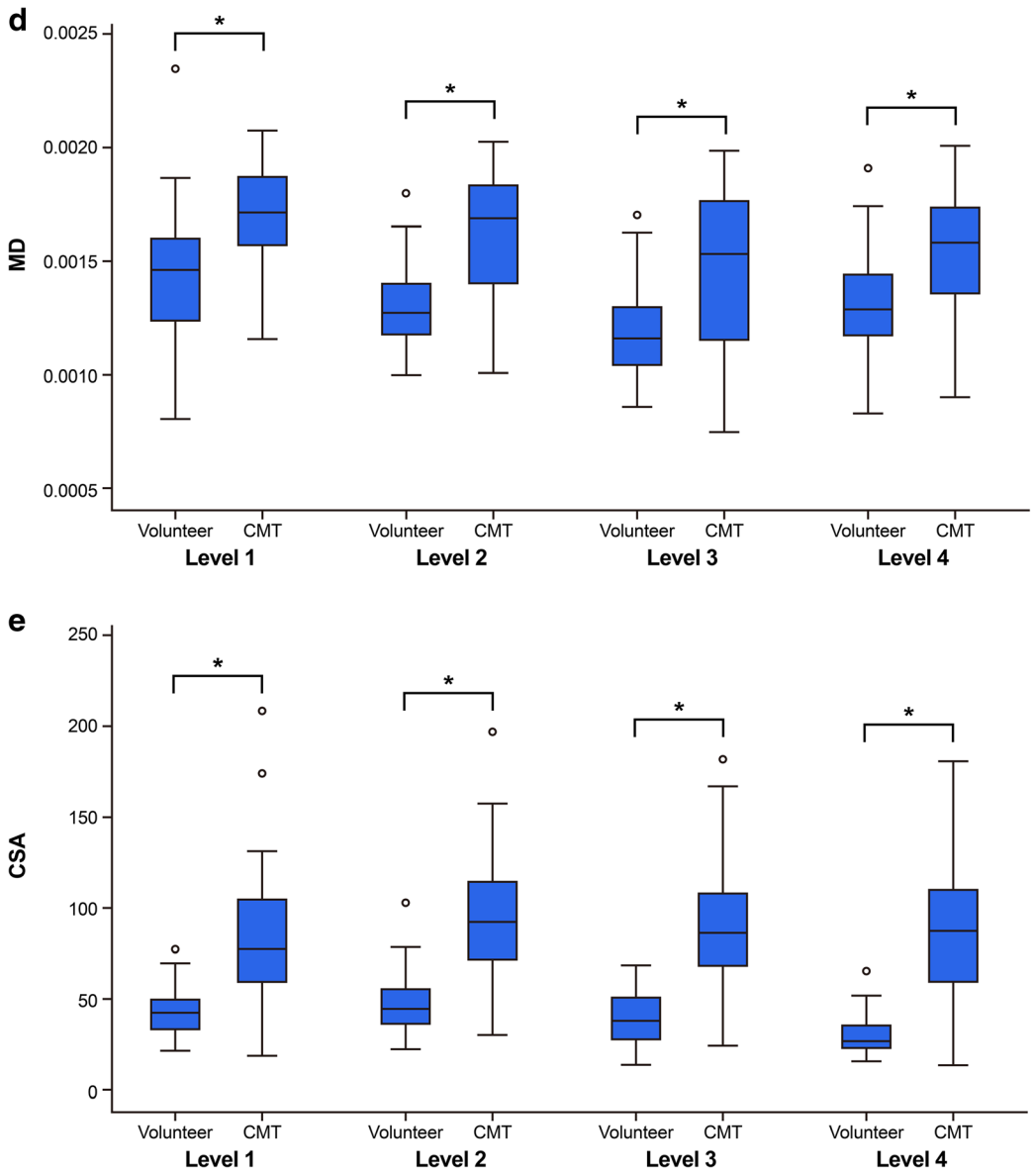

Fig. 3 (continued)

Because of the invasiveness and sequelae related to nerve biopsy, histologic correlation of parameters in the imaging study of nerve structure is very difficult. In this regard, CMT patients are appropriate cases for studying the DTI parameters because the disease typically involves the bilateral sciatic nerves, which are symmetrical in nature. We enrolled only CMT type I patients to examine the correlation of DTI parameters with demyelinating neuropathy. Furthermore, CMT type I has been reported as the most common type of CMT in most related studies [24]. In addition, we only included CMT patients in their 20s and 30s of age. This may have introduced some selection bias. However, we considered that it would be more meaningful, with regard to investigating the ability of DTI parameters, to perform the comparison study between the relatively early stage of CMT patients and their controls than performing comparison between patients with far advanced stage of the disease and controls.

Peripheral nerve pathology is reported to result in decreased FA and increased MD regardless of the type of underlying pathophysiology (e.g., axonal or demyelinating) in peripheral nerves [25–27]. Some recent studies have suggested a link between FA values and the demyelination process [25, 28, 29]. Recent studies conducted on median nerves have reported that FA values are significantly correlated with electrophysiologic markers of myelin sheath integrity [25, 28]. Kakuda et al. [29] also reported significantly lower FA values of tibial nerves in patients with chronic inflammatory demyelinating polyradiculoneuropathy (CIDP), the pathologic hallmark

Table 3 Receiver operating characteristic analysis results for diffusion tensor imaging parameters and cross-sectional area in differentiating the sciatic nerves of healthy controls and Charcot–Marie–Tooth disease patients

	AUC (95% CI)	Optimal cutoff	Sensitivity	Specificity	PPV	NPV	Accuracy
FA							
Level 1	0.921 (0.846–0.997)	0.478	0.944	0.900	0.919	0.931	0.924
Level 2	0.915 (0.847–0.982)	0.435	0.833	0.900	0.909	0.818	0.864
Level 3	0.845 (0.754–0.937)	0.455	0.639	0.967	0.958	0.690	0.788
Level 4	0.764 (0.642–0.886)	0.559	0.806	0.700	0.763	0.750	0.758
AD							
Level 2	0.651 (0.516–0.786)	2.398×10^{-3}	0.444	0.900	0.842	0.574	0.652
RD							
Level 1	0.865 (0.771–0.959)	1.222×10^{-3}	0.750	0.867	0.871	0.743	0.803
Level 2	0.865 (0.774–0.956)	1.036×10^{-3}	0.833	0.833	0.857	0.806	0.833
Level 3	0.790 (0.680–0.900)	1.053×10^{-3}	0.611	0.933	0.917	0.667	0.758
Level 4	0.761 (0.643–0.879)	0.955×10^{-3}	0.778	0.700	0.757	0.724	0.742
MD							
Level 1	0.787 (0.675–0.899)	1.564×10^{-3}	0.806	0.667	0.744	0.741	0.742
Level 2	0.815 (0.708–0.921)	1.395×10^{-3}	0.806	0.733	0.784	0.759	0.773
Level 3	0.702 (0.571–0.834)	1.516×10^{-3}	0.556	0.900	0.870	0.628	0.712
Level 4	0.740 (0.616–0.863)	1.350×10^{-3}	0.833	0.633	0.732	0.760	0.742
CSA							
Level 1	0.862 (0.768–0.955)	50.0	0.861	0.767	0.816	0.821	0.818
Level 2	0.875 (0.786–0.963)	64.0	0.861	0.833	0.861	0.833	0.848
Level 3	0.932 (0.863–1.000)	63.1	0.889	0.933	0.941	0.875	0.909
Level 4	0.922 (0.843–1.000)	54.7	0.861	0.967	0.969	0.853	0.909

FA fractional anisotropy, *AUC* area under the curve, *CI* confidence interval, *PPV* positive predictive value, *NPV* negative predictive value, *AD* axial diffusivity, *RD* radial diffusivity, *MD* mean diffusivity, *CSA* cross-sectional area

of which is also the loss of the myelin sheath. Kronlage et al. [14] also reported significantly lower FA in CIDP patients, which also showed strong correlation with electrophysiologic markers. Our study results are in agreement with those of the aforementioned studies.

Numerous studies on the central nervous system have suggested AD and RD as DTI parameters reflecting axonal and myelin sheath integrity, respectively [17, 30, 31]. Compared with DTI application to the central nervous system, DTI application to the peripheral nervous system is relatively new, and fewer related studies have been conducted. A recent study by Heckel et al. [28] showed a significant correlation of AD and RD with the electrophysiological parameters of axon and myelin sheath integrity, respectively, in the median nerve. Our study results showing CMT type I patients with significantly higher RD at all measured levels of the sciatic nerve are in agreement with these previous reports. These results suggest that RD may be a promising marker that indicated a demyelinating lesion of the peripheral nerves. Because MD is a mathematical combination of AD and RD, MD was also significantly higher in CMT patients, likely reflecting the RD profile. In addition to demyelination, other histologic changes, including increased fatty interfascicular epineurium, occur in the peripheral nerves of CMT patients [7, 32], but their contribution to changes in DTI parameters has not been investigated.

AD was significantly higher at level 2 in CMT patients than in normal controls. A decrease of AD, the diffusion of water parallel to nerve fibers, has been reported to indicate axonal damage [16, 33]. A previous study suggested that increased AD may be attributable to increased extra-axonal space resulting from the reduced axonal caliber of axonal density, which allows faster water molecule movement parallel to axons [34]. The difference in AD observed at one of the four measured levels could imply true histologic difference, but it may only be a result of the exceptionally sensitive nature of DTI. Further investigation is necessary to elucidate its true meaning.

In our study, multiple DTI parameters were measured in the sciatic nerves at various levels. The performance of each parameter may be considered promising, and these results warrant further studies on the clinical application of DTI in peripheral nerve evaluation. The cutoff values of DTI parameters with their diagnostic performance for discriminating normal

and demyelinated sciatic nerves at various levels may be used as reference values for future studies. However, DTI parameters are dependent on acquisition techniques and parameters [35]. Thus, the cutoff values provided in our study should be interpreted and applied with caution.

A recent study reported by Vaeggemose et al. [36] showed significantly lower FA and higher MD in the sciatic nerve of CMT type I patients compared with those of controls. In this study, DTI was performed at the distal sciatic nerve (10% of the distance from the upper part of the patella to the greater trochanter) without analysis of AD and RD. Our study demonstrated a significant difference of multiple DTI parameters including AD and RD in the sciatic nerves of proximal and mid-femur levels, which were not evaluated in previous studies. In addition, we also provided cutoff values of DTI parameters with their diagnostic performance for discriminating normal and pathologic sciatic nerves, and the study of Vaeggemose et al. [36] did not analyze. Furthermore, the patient and volunteer groups in the study of Vaeggemose et al. were not age-matched, which may have affected the FA value that is reported to be age-dependent [37]. In our study, the patient and control groups were age- and sex-matched for comparison.

The DTI analysis of the sciatic nerve at various levels in our study showed high inter-rater reproducibility. Wada et al. [20] reported excellent interobserver agreement in DTI analysis in their recent study on the proximal sciatic nerve. They used the fiber tracking method for measurement of the FA and MD of the sciatic nerve. In our study, the fiber tracking method was not used and ROIs were manually drawn pixel-by-pixel based on visual assessment, which resulted in excellent interobserver agreement. High inter-rater reproducibility was also observed in the measurement of the sciatic nerve at the mid-femur (level 4), where the caliber of the sciatic nerve is generally smaller than proximal segments.

Our results revealed significantly larger sciatic nerve CSAs in the CMT patients compared with previous reports [7]. This may represent the histopathologic features of CMT, such as loss of myelination or endoneurial fibrosis [7, 32]. However, to the best of our knowledge, little has been reported on the cutoff value of the sciatic nerve CSA for discriminating CMT patients and normal controls when measured at various levels. A recently published study by Kronlage et al. [38] showed significantly higher CSA of both the tibial and fibular portions of the sciatic nerves measured at the mid-thigh level in CIDP patients. In our study, we did not separately measure the tibial and fibular portions of the sciatic nerves and the levels where the measurements were performed also differ from the study of Kronlage et al. [38]. Data regarding sciatic nerve CSA of normal subjects from both studies may serve as a reference for future studies. Additional studies may prove the value of the sciatic nerve CSA in diagnosing CMT when used in conjunction with other MRI parameters.

After the evaluation of DTI image quality, the image sets of three patients were excluded. Clinical application of peripheral nerve DTI has been challenged because of its susceptibility to imaging artifacts associated with magnetic field inhomogeneity, incomplete fat suppression, aliasing, motion, and distortion [39, 40]. Because DTI was originally developed for the central nervous system, the development of dedicated sequences and postprocessing techniques may be necessary to help overcome these potential obstacles [40].

Our study had several limitations. First, the number of enrolled patients was small; however, we used an age- and sex-matched control group for comparison. Second, the clinical correlation between neurologic symptoms and imaging parameters was not tested. Third, measurement errors may have occurred in the analysis without using image co-registration between anatomical images and DTI, particularly in the distal sciatic nerve where the caliber is small. However, the significant difference observed between the two groups was similar to that observed at other levels. Fourth, the general application of cutoff values in our study may have been limited considering that MRI parameters may have affected the quantitative parameters. No general consensus exists on the optimal *b* value or the number of diffusion gradient directions for peripheral nerve DTI [40]. Considering the previous reports that using more than six diffusion directions improves the measurement of diffusion tensor [41, 42], six diffusion directions used in our study may not have been sufficient for exact evaluation of the diffusion parameters. Furthermore, a difference in slice thickness has been suggested as a factor affecting DTI parameters by introducing the partial volume effect [29]. Since a single axial image was used for analysis at each level rather than averaging the data acquired from multiple consecutive images, this may also have introduced partial volume effect. Lastly, signal-to-noise ratios (SNRs) of DTIs were not calculated. For exact SNR measurement in the parallel imaging, noise-only data should have been acquired through image scan without radiofrequency pulses to measure the exact noise [43], but these were not obtained in our study.

In conclusion, DTI assessment of the sciatic nerve is reproducible and has a potential value in discriminating the demyelinating nerve pathology of CMT type I patients from normal patients. The CSA of the sciatic nerve is also a potential quantitative parameter for diagnosing nerve abnormality in CMT type I patients. Cutoff values of each parameter reported in our study may be used as a reference for future studies, but they should be interpreted with caution considering the MRI acquisition parameters and anatomical locations. Additional studies are required to investigate potential applications of DTI in other types of demyelinating peripheral nerve pathology.

Funding This study has received funding by Bracco Imaging (PHO0162171).

Compliance with ethical standards

Guarantor The scientific guarantor of this publication is Young Cheol Yoon.

Conflict of interest The authors declare that they have no conflict of interest.

Statistics and biometry Insuk Sohn and Hyeseung Kim, the staffs of Bioinformatics Center, kindly provided statistical advice for this manuscript.

Informed consent Written informed consent was obtained from all subjects (patients) in this study.

Ethical approval Institutional review board approval was obtained.

Methodology
- prospective
- case–control study
- performed at one institution

References

1. Pareyson D, Marchesi C (2009) Diagnosis, natural history, and management of Charcot-Marie-Tooth disease. Lancet Neurol 8: 654–667
2. Bird TD, Ott J, Giblett ER, Chance PF, Sumi SM, Kraft GH (1983) Genetic linkage evidence for heterogeneity in Charcot-Marie-Tooth neuropathy (HMSN type I). Ann Neurol 14:679–684
3. Harding AE, Thomas PK (1980) The clinical features of hereditary motor and sensory neuropathy types I and II. Brain 103:259–280
4. Cornett KMD, Menezes MP, Shy RR et al (2017) Natural history of Charcot-Marie-Tooth disease during childhood. Ann Neurol 82: 353–359
5. Martinoli C, Schenone A, Bianchi S et al (2002) Sonography of the median nerve in Charcot-Marie-Tooth disease. AJR Am J Roentgenol 178:1553–1556
6. Noto Y, Shiga K, Tsuji Y et al (2015) Nerve ultrasound depicts peripheral nerve enlargement in patients with genetically distinct Charcot-Marie-Tooth disease. J Neurol Neurosurg Psychiatry 86: 378–384
7. Thawait SK, Chaudhry V, Thawait GK et al (2011) High-resolution MR neurography of diffuse peripheral nerve lesions. AJNR Am J Neuroradiol 32:1365–1372
8. Morano JU, Russell WF (1986) Nerve root enlargement in Charcot-Marie-Tooth disease: CT appearance. Radiology 161:784
9. Chung KW, Suh BC, Shy ME et al (2008) Different clinical and magnetic resonance imaging features between Charcot-Marie-Tooth disease type 1A and 2A. Neuromuscul Disord 18:610–618
10. Gaeta M, Mileto A, Mazzeo A et al (2012) MRI findings, patterns of disease distribution, and muscle fat fraction calculation in five patients with Charcot-Marie-Tooth type 2 F disease. Skeletal Radiol 41:515–524
11. Gallardo E, Claeys KG, Nelis E et al (2008) Magnetic resonance imaging findings of leg musculature in Charcot-Marie-Tooth disease type 2 due to dynamin 2 mutation. J Neurol 255:986–992
12. Morrow JM, Sinclair CD, Fischmann A et al (2016) MRI biomarker assessment of neuromuscular disease progression: a prospective observational cohort study. Lancet Neurol 15:65–77
13. Le Bihan D, Mangin JF, Poupon C et al (2001) Diffusion tensor imaging: concepts and applications. J Magn Reson Imaging 13: 534–546
14. Kronlage M, Schwehr V, Schwarz D et al (2018) Peripheral nerve diffusion tensor imaging (DTI): normal values and demographic determinants in a cohort of 60 healthy individuals. Eur Radiol 28: 1801–1808
15. Basser PJ, Pierpaoli C (1996) Microstructural and physiological features of tissues elucidated by quantitative-diffusion-tensor MRI. J Magn Reson B 111:209–219
16. Song SK, Sun SW, Ju WK, Lin SJ, Cross AH, Neufeld AH (2003) Diffusion tensor imaging detects and differentiates axon and myelin degeneration in mouse optic nerve after retinal ischemia. Neuroimage 20:1714–1722
17. Song SK, Sun SW, Ramsbottom MJ, Chang C, Russell J, Cross AH (2002) Dysmyelination revealed through MRI as increased radial (but unchanged axial) diffusion of water. Neuroimage 17:1429–1436
18. Budde MD, Xie M, Cross AH, Song SK (2009) Axial diffusivity is the primary correlate of axonal injury in the experimental autoimmune encephalomyelitis spinal cord: a quantitative pixelwise analysis. J Neurosci 29:2805–2813
19. Eguchi Y, Ohtori S, Orita S et al (2011) Quantitative evaluation and visualization of lumbar foraminal nerve root entrapment by using diffusion tensor imaging: preliminary results. AJNR Am J Neuroradiol 32:1824–1829
20. Wada K, Hashimoto T, Miyagi R, Sakai T, Sairyo K (2017) Diffusion tensor imaging and tractography of the sciatic nerve: assessment of fractional anisotropy and apparent diffusion coefficient values relative to the piriformis muscle, a preliminary study. Skeletal Radiol 46:309–314
21. Shi Y, Zong M, Xu X et al (2015) Diffusion tensor imaging with quantitative evaluation and fiber tractography of lumbar nerve roots in sciatica. Eur J Radiol 84:690–695
22. Budzik JF, Balbi V, Verclytte S, Pansini V, Le Thuc V, Cotten A (2014) Diffusion tensor imaging in musculoskeletal disorders. Radiographics 34:E56–E72
23. Delaney H, Bencardino J, Rosenberg ZS (2014) Magnetic resonance neurography of the pelvis and lumbosacral plexus. Neuroimaging Clin N Am 24:127–150
24. Barreto LC, Oliveira FS, Nunes PS et al (2016) Epidemiologic study of Charcot-Marie-Tooth disease: a systematic review. Neuroepidemiology 46:157–165
25. Bäumer P, Pham M, Ruetters M et al (2014) Peripheral neuropathy: detection with diffusion-tensor imaging. Radiology 273:185–193
26. Morisaki S, Kawai Y, Umeda M et al (2011) In vivo assessment of peripheral nerve regeneration by diffusion tensor imaging. J Magn Reson Imaging 33:535–542
27. Eppenberger P, Andreisek G, Chhabra A (2014) Magnetic resonance neurography: diffusion tensor imaging and future directions. Neuroimaging Clin N Am 24:245–256
28. Heckel A, Weiler M, Xia A et al (2015) Peripheral nerve diffusion tensor imaging: assessment of axon and myelin sheath integrity. PLoS One 10:e0130833
29. Kakuda T, Fukuda H, Tanitame K et al (2011) Diffusion tensor imaging of peripheral nerve in patients with chronic inflammatory demyelinating polyradiculoneuropathy: a feasibility study. Neuroradiology 53:955–960
30. Wozniak JR, Lim KO (2006) Advances in white matter imaging: a review of in vivo magnetic resonance methodologies and their

applicability to the study of development and aging. Neurosci Biobehav Rev 30:762–774
31. Song SK, Yoshino J, Le TQ et al (2005) Demyelination increases radial diffusivity in corpus callosum of mouse brain. Neuroimage 26:132–140
32. Smith TW, Bhawan J, Keller RB, DeGirolami U (1980) Charcot-Marie-Tooth disease associated with hypertrophic neuropathy: a neuropathologic study of two cases. J Neuropathol Exp Neurol 39:420–440
33. Loy DN, Kim JH, Xie M, Schmidt RE, Trinkaus K, Song SK (2007) Diffusion tensor imaging predicts hyperacute spinal cord injury severity. J Neurotrauma 24:979–990
34. Kumar R, Macey PM, Woo MA, Alger JR, Harper RM (2008) Diffusion tensor imaging demonstrates brainstem and cerebellar abnormalities in congenital central hypoventilation syndrome. Pediatr Res 64:275–280
35. Oudeman J, Nederveen AJ, Strijkers GJ, Maas M, Luijten PR, Froeling M (2016) Techniques and applications of skeletal muscle diffusion tensor imaging: a review. J Magn Reson Imaging 43:773–788
36. Vaeggemose M, Vaeth S, Pham M et al (2017) Magnetic resonance neurography and diffusion tensor imaging of the peripheral nerves in patients with Charcot-Marie-Tooth type 1A. Muscle Nerve 56: E78–E84
37. Tanitame K, Iwakado Y, Akiyama Y et al (2012) Effect of age on the fractional anisotropy (FA) value of peripheral nerves and clinical significance of the age-corrected FA value for evaluating polyneuropathies. Neuroradiology 54:815–821
38. Kronlage M, Baumer P, Pitarokoili K et al (2017) Large coverage MR neurography in CIDP: diagnostic accuracy and electrophysiological correlation. J Neurol 264:1434–1443
39. Johnson D, Stevens KJ, Riley G, Shapiro L, Yoshioka H, Gold GE (2015) Approach to MR imaging of the elbow and wrist: technical aspects and innovation. Magn Reson Imaging Clin N Am 23:355–366
40. Jeon T, Fung MM, Koch KM, Tan ET, Sneag DB (2018) Peripheral nerve diffusion tensor imaging: overview, pitfalls, and future directions. J Magn Reson Imaging 47:1171–1189
41. Papadakis NG, Murrills CD, Hall LD, Huang CL, Adrian Carpenter T (2000) Minimal gradient encoding for robust estimation of diffusion anisotropy. Magn Reson Imaging 18:671–679
42. Yao X, Yu T, Liang B, Xia T, Huang Q, Zhuang S (2015) Effect of increasing diffusion gradient direction number on diffusion tensor imaging fiber tracking in the human brain. Korean J Radiol 16:410–418
43. Kellman P, McVeigh ER (2005) Image reconstruction in SNR units: a general method for SNR measurement. Magn Reson Med 54: 1439–1447